



Observation of the mass difference between neutral charm-meson eigenstates

LHCb collaboration[†]

Abstract

A measurement of mixing and CP violation in neutral charm mesons is performed using data reconstructed in proton–proton collisions collected by the LHCb experiment from 2016 to 2018, corresponding to an integrated luminosity of 5.4 fb^{-1} . A total of 30.6 million $D^0 \rightarrow K_S^0 \pi^+ \pi^-$ decays are analyzed using a method optimized for the measurement of the mass difference between neutral charm-meson eigenstates. Allowing for CP violation in mixing and in the interference between mixing and decay, the mass and decay-width differences are measured to be $x_{CP} = [3.97 \pm 0.46 \text{ (stat)} \pm 0.29 \text{ (syst)}] \times 10^{-3}$ and $y_{CP} = [4.59 \pm 1.20 \text{ (stat)} \pm 0.85 \text{ (syst)}] \times 10^{-3}$, respectively. The CP -violating parameters are measured as $\Delta x = [-0.27 \pm 0.18 \text{ (stat)} \pm 0.01 \text{ (syst)}] \times 10^{-3}$ and $\Delta y = [0.20 \pm 0.36 \text{ (stat)} \pm 0.13 \text{ (syst)}] \times 10^{-3}$. This is the first observation of a nonzero mass difference in the D^0 meson system, with a significance exceeding seven standard deviations. The data are consistent with CP symmetry, and improve existing constraints on the associated parameters.

Submitted to Phys. Rev. Lett.

© 2022 CERN for the benefit of the LHCb collaboration. CC BY 4.0 licence.

[†]Authors are listed at the end of this paper.

Neutral charm mesons propagating freely can change (oscillate) into their own antiparticles, as the mass eigenstates are linear combinations of the flavor eigenstates. These flavor-changing neutral currents do not occur at tree level in the Standard Model (SM), and allow for hypothetical particles of arbitrarily high mass to contribute significantly to the process. This can affect the mixing of mesons and antimesons and probes physics beyond the SM [1].

The mass eigenstates of charm mesons can be written as $|D_{1,2}\rangle \equiv p|D^0\rangle \pm q|\bar{D}^0\rangle$, where p and q are complex parameters. Mixing of flavor eigenstates is described by the dimensionless parameters $x \equiv (m_1 - m_2)c^2/\Gamma$ and $y \equiv (\Gamma_1 - \Gamma_2)/(2\Gamma)$, where $m_{1(2)}$ and $\Gamma_{1(2)}$ are the mass and decay width of the $D_{1(2)}$ state, respectively, and Γ is the average decay width [2]. In D^0 and \bar{D}^0 decays to a common final state, f , CP violation in mixing manifests itself if $|q/p| \neq 1$ or in the interference between mixing and decay if $\phi_f \equiv \arg(q\bar{A}_f/pA_f) \neq 0$. Here A_f (\bar{A}_f) denotes the amplitude of the decay process $D^0 \rightarrow f$ ($\bar{D}^0 \rightarrow f$). In the $D^0 \rightarrow K_S^0\pi^+\pi^-$ decay studied in this Letter, CP violation in the decay ($|A_f|^2 \neq |\bar{A}_f|^2$) is not considered, as in the SM it is negligible for the doubly Cabibbo-suppressed (DCS) and Cabibbo-favored (CF) amplitudes contributing to this process. With this assumption, the CP -violating phase is independent of the final state, $\phi_f \approx \phi \approx \arg(q/p)$ [3].

The current world-average of the mixing and CP -violating parameters yields $x = (3.7 \pm 1.2) \times 10^{-3}$, $y = (6.8_{-0.7}^{+0.6}) \times 10^{-3}$, $|q/p| = 0.951_{-0.042}^{+0.053}$, and $\phi = -0.092_{-0.079}^{+0.085}$ [4]. Measurements using decays such as $D^0 \rightarrow K^+\pi^-$ have resulted in precise measurements of y and have allowed for the observation of mixing [4]. However, the data remains marginally compatible with $x = 0$, and is consistent with CP symmetry. Theoretical predictions for the mixing parameters are of similar magnitude but less precise, while predictions of the CP -violating phase are around 0.002 [3] and are well below the current experimental precision.

Sensitivity to the mixing and CP -violating parameters is offered by the self-conjugate, multibody $D^0 \rightarrow K_S^0\pi^+\pi^-$ decay [5–9]. Inclusion of the charge-conjugate process is implied unless stated otherwise. The dynamics of the decay are expressed as a function of two invariant masses following the Dalitz-plot formalism, in which a three-body decay is parameterized by a pair of two-body invariant masses [10, 11]. The squared invariant mass $m^2(K_S^0\pi^\pm)$ is denoted as m_\pm^2 for D^0 decays and m_\mp^2 for \bar{D}^0 decays. A mixture of DCS and CF decay amplitudes results in large variations of the strong phase and, with mixing, causes a decay-time evolution of the density of decays across the phase space. A joint analysis of the Dalitz-plot and decay-time distributions may be used to determine the mixing parameters. Splitting the sample by flavor of the charm meson at production probes for CP -violating effects. Usage of multibody decay modes is typically challenging, as it requires knowledge of the variation of the hadronic parameters and excellent control of efficiencies, resolutions, and background effects.

This Letter reports on a measurement of the mixing and CP violation parameters in $D^0 \rightarrow K_S^0\pi^+\pi^-$ decays using the “bin-flip” method [12], a model-independent approach which obviates the need for detailed models of the efficiency, resolution, and contributing amplitudes. Mixing and CP violation are parameterized by z_{CP} and Δz , which are defined by $z_{CP} \pm \Delta z \equiv -(q/p)^{\pm 1}(y+ix)$. The results are expressed in terms of the CP -even mixing parameters $x_{CP} \equiv -\text{Im}(z_{CP})$ and $y_{CP} \equiv -\text{Re}(z_{CP})$, and of the CP -violating differences $\Delta x \equiv -\text{Im}(\Delta z)$ and $\Delta y \equiv -\text{Re}(\Delta z)$. Conservation of CP symmetry implies $x_{CP} = x$, $y_{CP} = y$, and $\Delta x = \Delta y = 0$. The method has already been employed by the LHCb

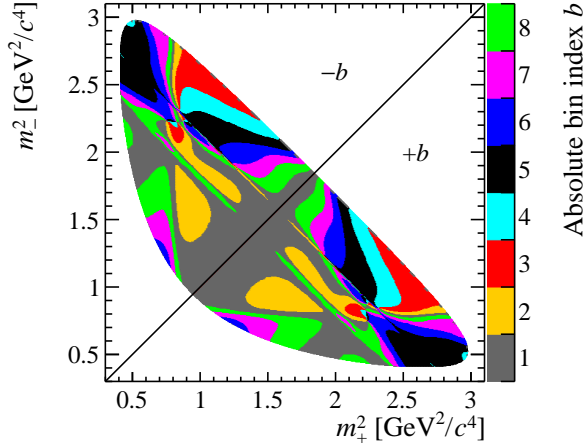


Figure 1: “Binning” of the $D^0 \rightarrow K_S^0 \pi^+ \pi^-$ Dalitz plot. Colors indicate the absolute value of the bin index b .

collaboration, yielding the single most precise measurement of x_{CP} and Δx [9].

In the bin-flip method, data are partitioned into disjoint regions (bins) of the Dalitz plot, which are defined to preserve nearly constant strong-phase differences $\Delta\delta(m_-^2, m_+^2)$ between the D^0 and \bar{D}^0 amplitudes within each bin [13]. Two sets of eight bins are formed symmetrically about the $m_+^2 = m_-^2$ bisector, as illustrated in Fig. 1. The region satisfying $m_+^2 > m_-^2$, which includes regions dominated by the CF $D^0 \rightarrow K^*(892)^- \pi^+$ decay, is given a positive index $+b$, while the opposite region, where the relative contribution from decays following an oscillation is enhanced, is given a negative index $-b$. The data are further split into 13 bins of decay time, chosen such that the bins are approximately equally populated. The squared-mass and decay-time resolutions are typically $0.006 \text{ GeV}^2/c^4$ and 60 fs, respectively, which are much smaller than the bin sizes used. Thus, they are neglected and accounted for in the systematic uncertainties.

For each decay-time interval (j), the ratio of the number of decays in each negative Dalitz-plot bin ($-b$) to its positive counterpart ($+b$) is measured. The usage of ratios minimizes the need for precise modeling of the efficiency variation across phase space and decay time. For small mixing parameters and CP -conserving decay amplitudes, the expected ratios for initially produced D^0 (\bar{D}^0) mesons, R_{bj}^+ (R_{bj}^-), are [12]

$$R_{bj}^\pm \approx \frac{r_b + r_b \frac{\langle t^2 \rangle_j}{4} \text{Re}(z_{CP}^2 - \Delta z^2) + \frac{\langle t^2 \rangle_j}{4} |z_{CP} \pm \Delta z|^2 + \sqrt{r_b} \langle t \rangle_j \text{Re}[X_b^*(z_{CP} \pm \Delta z)]}{1 + \frac{\langle t^2 \rangle_j}{4} \text{Re}(z_{CP}^2 - \Delta z^2) + r_b \frac{\langle t^2 \rangle_j}{4} |z_{CP} \pm \Delta z|^2 + \sqrt{r_b} \langle t \rangle_j \text{Re}[X_b(z_{CP} \pm \Delta z)]}. \quad (1)$$

The parameter r_b is the value of R_{bj} at $t = 0$, while X_b is the amplitude-weighted strong-phase difference between opposing bins. Finally, $\langle t \rangle_j$ ($\langle t^2 \rangle_j$) corresponds to the average (squared) decay time in each positive Dalitz-plot region where the mixed contribution is negligible, in units of the D^0 lifetime $\tau = \hbar/\Gamma$ [2], calculated directly from background-subtracted data. The other parameters are determined from a simultaneous fit of the observed R_{bj}^\pm ratios, in which external information on $c_b \equiv \text{Re}(X_b)$ and $s_b \equiv -\text{Im}(X_b)$ [13, 14] is used as a constraint.

Samples of $D^0 \rightarrow K_S^0 \pi^+ \pi^-$ decays are reconstructed from proton–proton (pp) collisions collected by the LHCb experiment from 2016 to 2018, corresponding to an integrated luminosity of 5.4 fb^{-1} . The strong-interaction decay $D^{*+} \rightarrow D^0 \pi^+$ is used to identify the flavor of the neutral charm meson at production. Throughout this Letter, D^{*+} indicates the $D^*(2010)^+$ meson and soft pion indicates the pion from its decay. The LHCb detector [15, 16] is a single-arm forward spectrometer covering the pseudorapidity range $2 < \eta < 5$, designed for the study of particles containing b or c quarks.

Decays of $K_S^0 \rightarrow \pi^+ \pi^-$ are reconstructed in two different categories: the first involving K_S^0 mesons that decay early enough for the pions to be reconstructed in all tracking detectors; and the second containing K_S^0 mesons that decay later such that track segments of the pions cannot be formed in the vertex detector, which surrounds the pp interaction (primary vertex) region, resulting in a worse momentum resolution. These categories are referred to as *long* and *downstream*, respectively. The downstream category contains more candidates but has slightly worse mass and decay-time resolution as well as larger efficiency variations.

The online event selection consists of a hardware stage, selecting events based on calorimeter and muon detector information, followed by two software stages. In the first software stage, the pion pair from the D^0 decay is required to satisfy criteria on momenta and final-state charged-particle displacements from any primary vertex for at least one pion (one-track) or both together with a vertex quality requirement (two-track). The second software stage fully reconstructs $D^{*+} \rightarrow D^0 \pi^+$, $D^0 \rightarrow K_S^0 \pi^+ \pi^-$ candidates using further requirements on particle identification, momenta, and track and vertex quality. Specific ranges of displacement and invariant mass are imposed on the reconstructed D^0 and K_S^0 candidates. Due to differing efficiencies, the sample is split into four categories, depending on whether they are *long* or *downstream* and whether or not they satisfy the one-track requirement.

Offline, a kinematic fit constrains the tracks to form vertices according to the decay topology, the K_S^0 candidate mass to the known value [2], and the D^{*+} candidate to a primary vertex [17]. In the reconstruction of the Dalitz-plot coordinates, an additional constraint on the D^0 candidate mass to the known value improves the resolution. Charm mesons originating from the decays of b hadrons are suppressed by requiring that the D^0 and soft pion candidates originate from a primary vertex. Candidates are rejected if two of the reconstructed tracks use the same hits in the vertex detector. About 6% of the candidates are from collision events in which multiple candidates are reconstructed, usually by pairing the same D^0 candidate with different soft pions. When this occurs, one candidate is chosen randomly, and the rest are removed from the sample.

Signal yields are determined by fitting the distribution of the mass difference between the D^{*+} and D^0 candidates, denoted as Δm . The signal probability density function is empirically described by a combination of a Johnson S_U distribution [18] and two Gaussian functions, one of which shares a mean with the Johnson S_U . The background is dominated by real D^0 decays incorrectly combined with a charged particle not associated with a D^{*+} decay, and is modeled with a smooth phase-space-like model, $\theta(\Delta m - m_\pi) e^{-c(\Delta m - m_\pi)} (\Delta m - m_\pi)^\alpha$, where $\theta(x)$ is the Heaviside step function, m_π is the charged-pion mass [2], and α and c are free parameters. Fig. 2 shows the Δm distribution of the entire sample, from which the fit identifies $(30.585 \pm 0.011) \times 10^6$ signal decays. This represents a factor of 15 larger yield compared to the previous measurement.

To determine the yields used to form the ratios R_{bj}^\pm , separate fits are performed for each

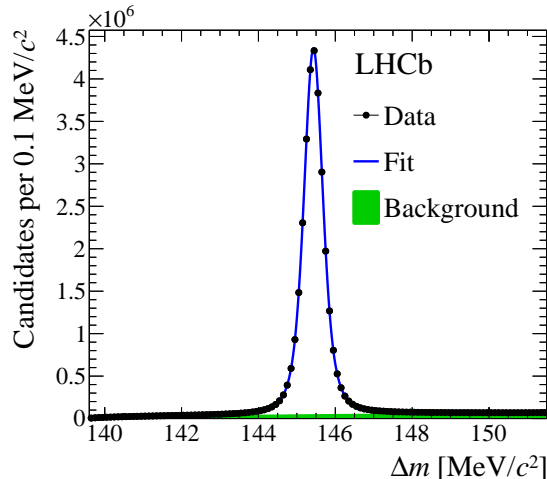


Figure 2: Distribution of Δm for the selected $D^{*+} \rightarrow D^0(\rightarrow K_S^0 \pi^+ \pi^-) \pi^+$ candidates. The projection of the fit result is superimposed.

set of Dalitz-plot and decay-time bins bj . The signal model assumes the same parameters for each pair of positive and negative Dalitz-plot bins, and fixes some parameters from a fit integrated over decay time. Fits are performed independently for D^0 and \bar{D}^0 candidates, as well as for each of the four data subsamples. The measured signal yields are then corrected for two effects that do not cancel in the ratio: experimentally induced correlations between the phase space and decay time, and charge-dependent efficiencies (detection asymmetries).

Online requirements on the displacement and momenta of the D^0 decay products introduce efficiency variations that are correlated between the phase-space coordinates and the D^0 decay time. The effect depends predominantly on the invariant mass of two pions from the D^0 decay, with the efficiency to reconstruct the candidates at low values decreasing significantly at low D^0 decay times. This can bias the measured yield ratios and produce mixing-like trends. To remove this bias, an approach which estimates the relative efficiencies using data is developed. The Dalitz plot is divided into small, rectangular-like regions formed symmetrically across the bisector. Note that these include the portions above and below the bisector, unlike the bins shown in Fig. 1. In the limit of CP symmetry, the contribution of mixing to such symmetric regions depends only on y_{CP} and the hadronic parameters of the D^0 decay [12]. As oscillations result in a migration of decays from one side of the Dalitz plot to the other, and the regions are symmetric with respect to the bisector, there is no effect from x_{CP} . Given a set of inputs for y_{CP} and the hadronic parameters, the contribution of mixing to the decay-time distributions of these regions can be accounted for, such that the remaining differences between regions come from the efficiency correlations. Relative efficiency maps which align the decay-time distributions in all these symmetric regions can then be calculated. Per-candidate weights assigned by the efficiency maps are integrated over the data in each bin using the sPlot method [19] with Δm as the discriminating variable. This provides correction factors for each of the fitted signal yields.

In calculating the efficiency maps, the strong phase variation within a Dalitz-plot bin is approximated as constant, such that it can be described by the external inputs (s_b). As y_{CP} and s_b are parameters of the fit, the correction maps and corresponding correction

factors are calculated for a range of values. The smallness of mixing results in smooth variations of the correction factors for a given Dalitz-plot bin, which allows for precise interpolation between the calculated points with polynomials. These polynomials are then incorporated into the fit as a correction which depends on y_{CP} and s_b . The correction is calculated for each yield ratio, but is averaged over the initial flavor of the candidates. The procedure has been validated with pseudoexperiments, and a systematic uncertainty is assigned due to the approximation that s_b is constant within a bin.

Corrections are also applied in order to take into account detection asymmetries. Due to utilizing ratios of yields, the analysis is insensitive to detection asymmetries of the K_S^0 , as well as the soft pion used to tag the flavor of the candidate. However, the kinematics of the pions produced in the D^0 decay depend on the Dalitz-plot coordinate and D^0 flavor. This can result in asymmetric efficiency variations for D^0 and \bar{D}^0 candidates that imitate CP violation. The two-track $\pi^+\pi^-$ asymmetry, $A_{\text{det}}(\pi^+\pi^-)$, is determined by measuring detection asymmetries in control samples of $D_s^+ \rightarrow \pi^+\pi^+\pi^-$ and $D_s^+ \rightarrow \phi\pi^+$ decays, in which the ϕ meson is reconstructed through a K^+K^- pair. A randomly chosen π^+ in the $D_s^+ \rightarrow \pi^+\pi^+\pi^-$ decay is paired with the π^- to form a proxy for the $\pi^+\pi^-$ pair of interest. The $D_s^+ \rightarrow \phi\pi^+$ sample is used to cancel asymmetries induced from the remaining π^+ , $A_{\text{det}}(\pi^+)$, and other sources, such as the trigger selection, $A_{\text{trigger}}(D_s^+)$, and the production of D_s^+ and D_s^- mesons in pp collisions, $A_{\text{prod}}(D_s^+)$. Specifically, the raw asymmetries A_{meas} can be written as

$$\begin{aligned} A_{\text{meas}}(D_s^+ \rightarrow \pi^+\pi^+\pi^-) &= A_{\text{det}}(\pi^+\pi^-) + A_{\text{det}}(\pi^+) + A_{\text{prod}}(D_s^+) + A_{\text{trigger}}(D_s^+), \\ A_{\text{meas}}(D_s^+ \rightarrow \phi\pi^+) &= A_{\text{det}}(\pi^+) + A_{\text{prod}}(D_s^+) + A_{\text{trigger}}(D_s^+). \end{aligned} \quad (2)$$

The difference of the two measured asymmetries gives the detection asymmetry of the $\pi^+\pi^-$ pair. The control samples are weighted to match the kinematics of the pions from the $D^0 \rightarrow K_S^0\pi^+\pi^-$ sample. This weighting is done separately for each Dalitz-plot bin. The detection asymmetries are of the order of 10^{-3} and are used as corrections to the measured yields. They are included as constraints in the fit along with the associated covariance matrix ΔV_{asym} describing uncertainties coming from the limited size of the calibration samples.

The mixing parameters are determined by minimizing a least-squares function

$$\begin{aligned} \chi^2 &\equiv \sum_{+,-} \sum_{b,j} \frac{[N_{-bj}^\pm - R_{+bj}^\pm N_{+bj}^\pm / (C_{bj}(1 \pm \Delta A_b))]^2}{(\sigma_{-bj}^\pm)^2 + [R_{+bj}^\pm \sigma_{+bj}^\pm / (C_{bj}(1 \pm \Delta A_b))]^2} \\ &+ \sum_{b,b'} (X_b^{\text{EXT}} - X_b) (V_{\text{EXT}}^{-1})_{bb'} (X_{b'}^{\text{EXT}} - X_{b'}) \\ &+ \sum_{b,b'} (\Delta A_b^{\text{asym}} - \Delta A_b) (\Delta V_{\text{asym}}^{-1})_{bb'} (\Delta A_{b'}^{\text{asym}} - \Delta A_{b'}), \end{aligned} \quad (3)$$

where the yields N and their measured uncertainties σ are scaled by factors for the correlation removal, C_{bj} , and detection asymmetry correction, $\Delta A^b \equiv A_{\text{det}}^b(\pi^+\pi^-) - A_{\text{det}}^{-b}(\pi^+\pi^-)$. The different subsamples are fitted simultaneously, separated between D^0 and \bar{D}^0 flavors denoted as $+$ and $-$, including all decay-time intervals j and Dalitz-plot bins b . The parameters X_b are constrained with a Gaussian penalty term using the values X_b^{EXT} and covariance matrix V_{EXT} from a combination of CLEO and BESIII measurements [13, 14]. In the fit, the parameters r_b are determined independently for

each subsample, as they are affected by the sample-specific variation of the efficiency over the Dalitz plot [12]. To avoid experimenter's bias, the values of x_{CP} , y_{CP} , Δx , and Δy were not examined until the full procedure had been finalized. Figure 3 shows the yield ratios with fit projections overlaid for each of the eight Dalitz-plot bins. Deviations from constant values are due to mixing. The fit projection when x_{CP} is fixed to zero is also included and shows the inability of a nonzero y_{CP} value to produce the deviations on its own. Also shown are the differences of ratios between D^0 and \bar{D}^0 decays, where a significant slope would indicate CP violation.

Systematic uncertainties are assessed from ensembles of pseudoexperiments. These use the $D^0 \rightarrow K_S^0 \pi^+ \pi^-$ model of Ref. [20] to describe the amplitude at $t = 0$, and the decay-time dependence is incorporated for a range of values of the mixing and CP violation parameters. Different sources of systematic uncertainty are included, and the effect on the measured parameters evaluated. The dominant systematic uncertainty on the mixing parameters comes from reconstruction and selection effects, and amounts to 0.20×10^{-3} (0.76×10^{-3}) for x_{CP} (y_{CP}). This includes neglecting the decay-time and m_{\pm}^2 resolutions and efficiencies, as well as the correction to remove the efficiency correlations. The most important effect for y_{CP} is the approximation of the strong phase to be constant within each bin in the procedure to remove correlations. Contamination from b -hadron decays contributes 0.20×10^{-3} (0.15×10^{-3}) to the x_{CP} (y_{CP}) uncertainty. Potential mismodeling in the signal yield fits contributes 0.36×10^{-3} to the y_{CP} uncertainty. Time-dependent detection asymmetries are mainly present in bins which give the best sensitivity to Δy , resulting in a systematic uncertainty of 0.12×10^{-3} .

The consistency of the results is tested by repeating the analysis in subsets of the data, divided according to magnet polarity, trigger and K_S^0 category, data-taking period, D^{*+} meson kinematics, and other categories. The largest variation occurs for the value of x_{CP} as a function of D^{*+} meson pseudorapidity, where the compatibility, considering statistical uncertainties only, amounts to a p-value of 1.5%, depending on the details of the sample split, whereas the overall p-value for all x_{CP} observed variations has a p-value above 8%. The observed variations of the observables x_{CP} , y_{CP} , Δx and Δy are all consistent with statistical fluctuations.

The mixing and CP violation parameters are measured to be

$$\begin{aligned} x_{CP} &= (3.97 \pm 0.46 \pm 0.29) \times 10^{-3}, \\ y_{CP} &= (4.59 \pm 1.20 \pm 0.85) \times 10^{-3}, \\ \Delta x &= (-0.27 \pm 0.18 \pm 0.01) \times 10^{-3}, \\ \Delta y &= (0.20 \pm 0.36 \pm 0.13) \times 10^{-3}, \end{aligned}$$

where the first uncertainty is statistical and the second systematic. The statistical uncertainty contains a subleading component due to the limited precision of the external measurements of the strong phases and control samples used for the detection asymmetry. This amounts to approximately $(0.23, 0.66, 0.04, \text{ and } 0.08) \times 10^{-3}$ for x_{CP} , y_{CP} , Δx , and Δy , respectively. The measurements are statistically limited, though the systematic uncertainty on y_{CP} is comparable to the statistical uncertainty. The results are used to form a likelihood function of x , y , $|q/p|$, and ϕ using a likelihood-ratio ordering that assumes the observed correlations to be independent of the true parameter values [21].

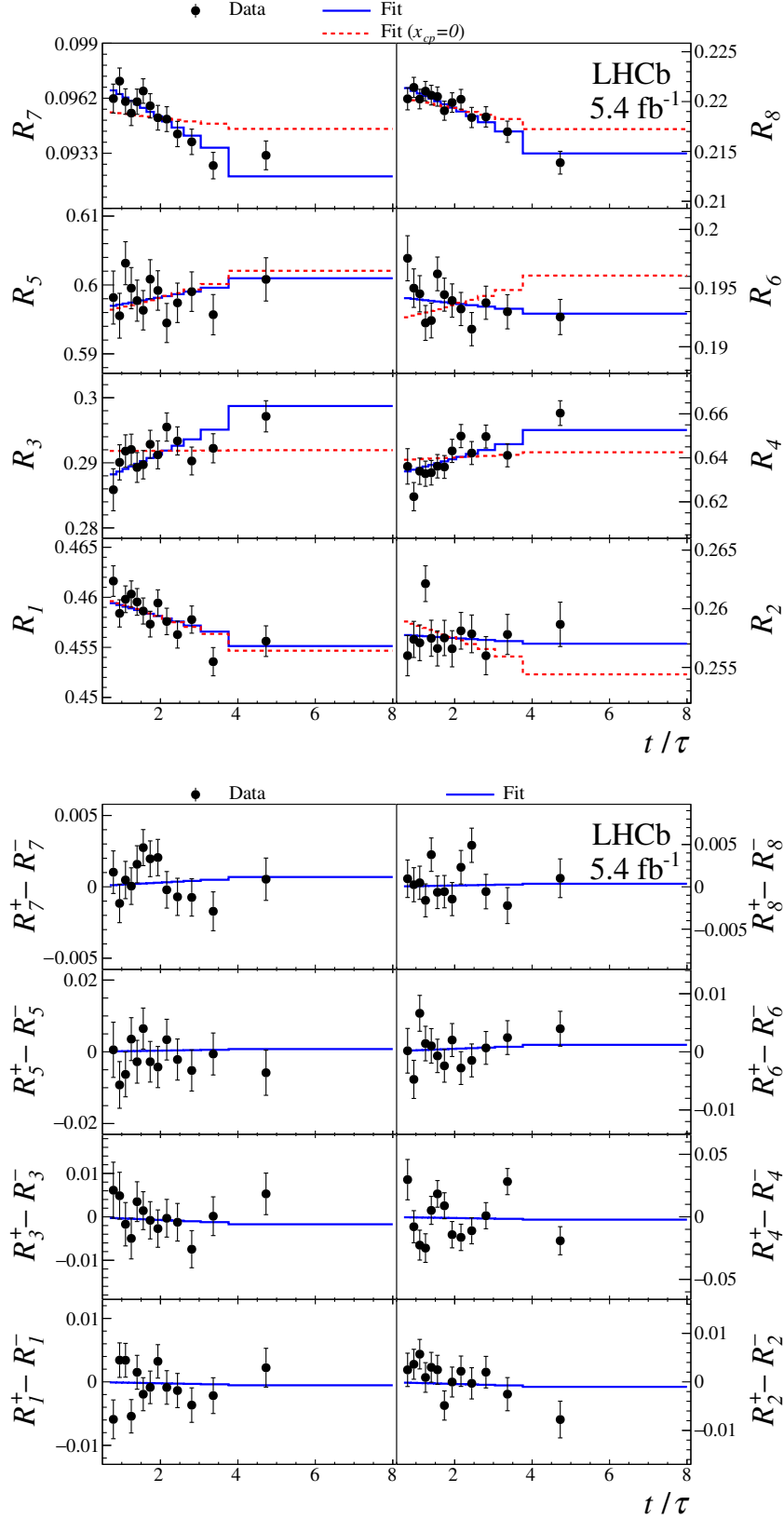


Figure 3: (Top) CP -averaged yield ratios and (bottom) differences of D^0 and \bar{D}^0 yield ratios as a function of t/τ , shown for each Dalitz-plot bin with fit projections overlaid.

The best fit point is

$$\begin{aligned}x &= (3.98^{+0.56}_{-0.54}) \times 10^{-3}, \\y &= (4.6^{+1.5}_{-1.4}) \times 10^{-3}, \\|q/p| &= 0.996 \pm 0.052, \\\phi &= 0.056^{+0.047}_{-0.051}.\end{aligned}$$

In summary, a measurement of mixing and CP violation in $D^0 \rightarrow K_S^0 \pi^+ \pi^-$ decays has been performed with the bin-flip method, using pp collision data collected by the LHCb experiment and corresponding to an integrated luminosity of 5.4 fb^{-1} . This resulted in the first observation of a nonzero value of the mass difference x of neutral charm meson mass eigenstates with a significance of more than seven standard deviations, and significantly improves limits on mixing-induced CP violation in the charm sector.

Acknowledgements

We express our gratitude to our colleagues in the CERN accelerator departments for the excellent performance of the LHC. We thank the technical and administrative staff at the LHCb institutes. We acknowledge support from CERN and from the national agencies: CAPES, CNPq, FAPERJ and FINEP (Brazil); MOST and NSFC (China); CNRS/IN2P3 (France); BMBF, DFG and MPG (Germany); INFN (Italy); NWO (Netherlands); MNiSW and NCN (Poland); MEN/IFA (Romania); MSHE (Russia); MICINN (Spain); SNSF and SER (Switzerland); NASU (Ukraine); STFC (United Kingdom); DOE NP and NSF (USA). We acknowledge the computing resources that are provided by CERN, IN2P3 (France), KIT and DESY (Germany), INFN (Italy), SURF (Netherlands), PIC (Spain), GridPP (United Kingdom), RRCKI and Yandex LLC (Russia), CSCS (Switzerland), IFIN-HH (Romania), CBPF (Brazil), PL-GRID (Poland) and NERSC (USA). We are indebted to the communities behind the multiple open-source software packages on which we depend. Individual groups or members have received support from ARC and ARDC (Australia); AvH Foundation (Germany); EPLANET, Marie Skłodowska-Curie Actions and ERC (European Union); A*MIDEX, ANR, IPhU and Labex P2IO, and Région Auvergne-Rhône-Alpes (France); Key Research Program of Frontier Sciences of CAS, CAS PIFI, CAS CCEPP, Fundamental Research Funds for the Central Universities, and Sci. & Tech. Program of Guangzhou (China); RFBR, RSF and Yandex LLC (Russia); GVA, XuntaGal and GENCAT (Spain); the Leverhulme Trust, the Royal Society and UKRI (United Kingdom).

References

- [1] G. Isidori, Y. Nir, and G. Perez, *Flavor physics constraints for physics beyond the standard model*, Ann. Rev. Nucl. Part. Sci. **60** (2010) 355, [arXiv:1002.0900](#).
- [2] Particle Data Group, P. A. Zyla *et al.*, *Review of particle physics*, to be published in Prog. Theor. Exp. Phys. **6** (2020) 083C01.
- [3] A. L. Kagan and L. Silvestrini, *Dispersive and absorptive CP violation in $D^0 - \bar{D}^0$ mixing*, Phys. Rev. D **103** (2021) 053008, [arXiv:2001.07207](#).

- [4] Heavy Flavor Averaging Group, Y. Amhis *et al.*, *Averages of b-hadron, c-hadron, and τ -lepton properties as of 2018*, arXiv:1909.12524, updated results and plots available at <https://hflav.web.cern.ch>.
- [5] CLEO collaboration, D. M. Asner *et al.*, *Search for D^0 - \bar{D}^0 mixing in the Dalitz plot analysis of $D^0 \rightarrow K_S^0 \pi^+ \pi^-$* , Phys. Rev. **D72** (2005) 012001, arXiv:hep-ex/0503045.
- [6] Belle collaboration, T. Peng *et al.*, *Measurement of D^0 - \bar{D}^0 mixing and search for indirect CP violation using $D^0 \rightarrow K_S^0 \pi^+ \pi^-$ decays*, Phys. Rev. **D89** (2014) 091103, arXiv:1404.2412.
- [7] BaBar collaboration, P. del Amo Sanchez *et al.*, *Measurement of D^0 - \bar{D}^0 mixing parameters using $D^0 \rightarrow K_S^0 \pi^+ \pi^-$ and $D^0 \rightarrow K_S^0 K^+ K^-$ decays*, Phys. Rev. Lett. **105** (2010) 081803, arXiv:1004.5053.
- [8] LHCb collaboration, R. Aaij *et al.*, *Model-independent measurement of mixing parameters in $D^0 \rightarrow K_S^0 \pi^+ \pi^-$ decays*, JHEP **04** (2016) 033, arXiv:1510.01664.
- [9] LHCb collaboration, R. Aaij *et al.*, *Measurement of the mass difference between neutral charm-meson eigenstates*, Phys. Rev. Lett. **122** (2019) 231802, arXiv:1903.03074.
- [10] R. H. Dalitz, *On the analysis of τ -meson data and the nature of the τ -meson*, Phil. Mag. Ser. 7 **44** (1953) 1068.
- [11] E. Fabri, *A study of τ -meson decay*, Nuovo Cim. **11** (1954) 479.
- [12] A. Di Canto *et al.*, *Novel method for measuring charm-mixing parameters using multibody decays*, Phys. Rev. **D99** (2019) 012007, arXiv:1811.01032.
- [13] CLEO collaboration, J. Libby *et al.*, *Model-independent determination of the strong-phase difference between D^0 and $\bar{D}^0 \rightarrow K_{S,L}^0 h^+ h^-$ ($h = \pi, K$) and its impact on the measurement of the CKM angle γ/ϕ_3* , Phys. Rev. **D82** (2010) 112006, arXiv:1010.2817.
- [14] BESIII collaboration, M. Ablikim *et al.*, *Model-independent determination of the relative strong-phase difference between D^0 and $\bar{D}^0 \rightarrow K_{S,L}^0 \pi^+ \pi^-$ and its impact on the measurement of the CKM angle γ/ϕ_3* , Phys. Rev. **D101** (2020) 112002, arXiv:2003.00091.
- [15] LHCb collaboration, A. A. Alves Jr. *et al.*, *The LHCb detector at the LHC*, JINST **3** (2008) S08005.
- [16] LHCb collaboration, R. Aaij *et al.*, *LHCb detector performance*, Int. J. Mod. Phys. **A30** (2015) 1530022, arXiv:1412.6352.
- [17] W. D. Hulsbergen, *Decay chain fitting with a Kalman filter*, Nucl. Instrum. Meth. **A552** (2005) 566, arXiv:physics/0503191.
- [18] N. L. Johnson, *Systems of frequency curves generated by methods of translation*, Biometrika **36** (1949) 149.

- [19] M. Pivk and F. R. Le Diberder, *sPlot: A statistical tool to unfold data distributions*, Nucl. Instrum. Meth. **A555** (2005) 356, [arXiv:physics/0402083](#).
- [20] BaBar collaboration, Belle collaboration, I. Adachi *et al.*, *First evidence for $\cos 2\beta > 0$ and resolution of the CKM Unitarity Triangle ambiguity by a time-dependent Dalitz plot analysis of $B^0 \rightarrow D^{(*)}h^0$ with $D \rightarrow K_S^0\pi^+\pi^-$ decays*, Phys. Rev. Lett. **121** (2018) 261801, [arXiv:1804.06152](#).
- [21] LHCb collaboration, R. Aaij *et al.*, *Measurement of the CKM angle γ from a combination of $B^\pm \rightarrow Dh^\pm$ analyses*, Phys. Lett. **B726** (2013) 151, [arXiv:1305.2050](#).

1 Supplemental material

Table 1 summarizes the measured values along with their uncertainties and correlations. Table 2 gives the derived values for x , y , q/p and ϕ together with the 95.5% confidence interval. Table 3 shows a summary of the uncertainties in this analysis. Fig. 4 shows the Dalitz plot of the background-subtracted $D^0 \rightarrow K_S^0 \pi^+ \pi^-$ candidates used in the analysis. No efficiency corrections are applied. All samples are combined.

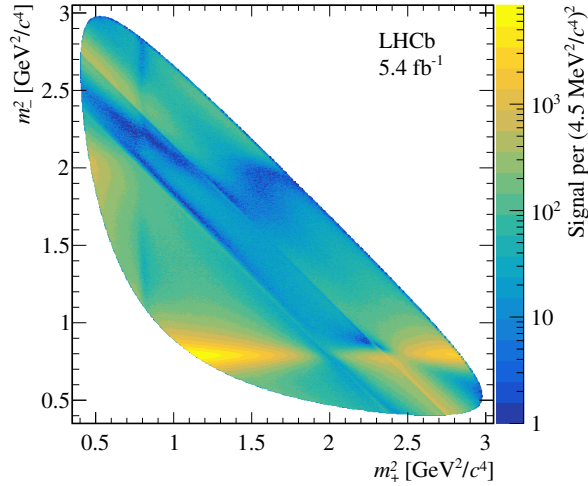


Figure 4: Dalitz plot of background-subtracted $D^0 \rightarrow K_S^0 \pi^+ \pi^-$ candidates.

Table 1: Fit results of x_{CP} , y_{CP} , Δx , and Δy . The first contribution to the uncertainty is statistical, the second systematic.

Parameter	Value [10^{-3}]	Stat. correlations			Syst. correlations		
		y_{CP}	Δx	Δy	y_{CP}	Δx	Δy
x_{CP}	$3.97 \pm 0.46 \pm 0.29$	0.11	-0.02	-0.01	0.13	0.01	0.01
y_{CP}	$4.59 \pm 1.20 \pm 0.85$		-0.01	-0.05		-0.02	0.01
Δx	$-0.27 \pm 0.18 \pm 0.01$			0.08			0.31
Δy	$0.20 \pm 0.36 \pm 0.13$						

Table 2: Point estimates and 95.5% confidence-level (CL) intervals for x , y , $|q/p|$ and ϕ . The uncertainties include statistical and systematic contributions.

Parameter	Value	95.5% CL interval
$x [10^{-3}]$	$3.98^{+0.56}_{-0.54}$	[2.9, 5.0]
$y [10^{-3}]$	$4.6^{+1.5}_{-1.4}$	[2.0, 7.5]
$ q/p $	0.996 ± 0.052	[0.890, 1.110]
ϕ	$-0.056^{+0.047}_{-0.051}$	[-0.172, 0.040]

Table 3: Uncertainties in units of 10^{-3} . The total systematic uncertainty is the sum in quadrature of the individual components. The uncertainties due to the external inputs and detection asymmetry calibration samples are included in the statistical uncertainty. These are also reported separately, along with the contributions due to the limited sample size, to ease comparison with other sources.

Source	x_{CP}	y_{CP}	Δx	Δy
Reconstruction and selection	0.199	0.757	0.009	0.044
Secondary charm decays	0.208	0.154	0.001	0.002
Detection asymmetry	0.000	0.001	0.004	0.102
Mass-fit model	0.045	0.361	0.003	0.009
Total systematic uncertainty	0.291	0.852	0.010	0.110
Strong phase inputs	0.23	0.66	0.02	0.04
Detection asymmetry inputs	0.00	0.00	0.04	0.08
Statistical (w/o inputs)	0.40	1.00	0.18	0.35
Total statistical uncertainty	0.46	1.20	0.18	0.36

LHCb collaboration

R. Aaij³², C. Abellán Beteta⁵⁰, T. Ackernley⁶⁰, B. Adeva⁴⁶, M. Adinolfi⁵⁴, H. Afsharnia⁹,
 C.A. Aidala⁸⁶, S. Aiola²⁵, Z. Ajaltouni⁹, S. Akar⁶⁵, J. Albrecht¹⁵, F. Alessio⁴⁸, M. Alexander⁵⁹,
 A. Alfonso Alberio⁴⁵, Z. Aliouche⁶², G. Alkhazov³⁸, P. Alvarez Cartelle⁵⁵, S. Amato²,
 Y. Amhis¹¹, L. An⁴⁸, L. Anderlini²², A. Andreianov³⁸, M. Andreotti²¹, F. Archilli¹⁷,
 A. Artamonov⁴⁴, M. Artuso⁶⁸, K. Arzymatov⁴², E. Aslanides¹⁰, M. Atzeni⁵⁰, B. Audurier¹²,
 S. Bachmann¹⁷, M. Bachmayer⁴⁹, J.J. Back⁵⁶, P. Baladron Rodriguez⁴⁶, V. Balagura¹²,
 W. Baldini²¹, J. Baptista Leite¹, R.J. Barlow⁶², S. Barsuk¹¹, W. Barter⁶¹, M. Bartolini²⁴,
 F. Baryshnikov⁸³, J.M. Basels¹⁴, G. Bassi²⁹, B. Batsukh⁶⁸, A. Battig¹⁵, A. Bay⁴⁹, M. Becker¹⁵,
 F. Bedeschi²⁹, I. Bediaga¹, A. Beiter⁶⁸, V. Belavin⁴², S. Belin²⁷, V. Bellee⁴⁹, K. Belous⁴⁴,
 I. Belov⁴⁰, I. Belyaev⁴¹, G. Bencivenni²³, E. Ben-Haim¹³, A. Berezhnoy⁴⁰, R. Bernet⁵⁰,
 D. Berninghoff¹⁷, H.C. Bernstein⁶⁸, C. Bertella⁴⁸, A. Bertolin²⁸, C. Betancourt⁵⁰, F. Betti⁴⁸,
 Ia. Bezshyiko⁵⁰, S. Bhasin⁵⁴, J. Bhom³⁵, L. Bian⁷³, M.S. Bieker¹⁵, S. Bifani⁵³, P. Billoir¹³,
 M. Birch⁶¹, F.C.R. Bishop⁵⁵, A. Bitadze⁶², A. Bizzeti^{22,k}, M. Bjørn⁶³, M.P. Blago⁴⁸, T. Blake⁵⁶,
 F. Blanc⁴⁹, S. Blusk⁶⁸, D. Bobulska⁵⁹, J.A. Boelhauve¹⁵, O. Boente Garcia⁴⁶, T. Boettcher⁶⁵,
 A. Boldyrev⁸², A. Bondar⁴³, N. Bondar^{38,48}, S. Borghi⁶², M. Borisyak⁴², M. Borsato¹⁷,
 J.T. Borsuk³⁵, S.A. Bouchiba⁴⁹, T.J.V. Bowcock⁶⁰, A. Boyer⁴⁸, C. Bozzi²¹, M.J. Bradley⁶¹,
 S. Braun⁶⁶, A. Brea Rodriguez⁴⁶, M. Brodski⁴⁸, J. Brodzicka³⁵, A. Brossa Gonzalo⁵⁶,
 D. Brundu²⁷, A. Buonaura⁵⁰, C. Burr⁴⁸, A. Bursche⁷², A. Butkevich³⁹, J.S. Butter³²,
 J. Buytaert⁴⁸, W. Byczynski⁴⁸, S. Cadeddu²⁷, H. Cai⁷³, R. Calabrese^{21,f}, L. Calefice^{15,13},
 L. Calero Diaz²³, S. Cali²³, R. Calladine⁵³, M. Calvi^{26,j}, M. Calvo Gomez⁸⁵,
 P. Camargo Magalhaes⁵⁴, P. Campana²³, A.F. Campoverde Quezada⁶, S. Capelli^{26,j},
 L. Capriotti^{20,d}, A. Carbone^{20,d}, G. Carboni³¹, R. Cardinale²⁴, A. Cardini²⁷, I. Carli⁴,
 P. Carniti^{26,j}, L. Carus¹⁴, K. Carvalho Akiba³², A. Casais Vidal⁴⁶, G. Casse⁶⁰, M. Cattaneo⁴⁸,
 G. Cavallero⁴⁸, S. Celani⁴⁹, J. Cerasoli¹⁰, A.J. Chadwick⁶⁰, M.G. Chapman⁵⁴, M. Charles¹³,
 Ph. Charpentier⁴⁸, G. Chatzikonstantinidis⁵³, C.A. Chavez Barajas⁶⁰, M. Chefdeville⁸,
 C. Chen³, S. Chen⁴, A. Chernov³⁵, V. Chobanova⁴⁶, S. Cholak⁴⁹, M. Chruszcz³⁵,
 A. Chubykin³⁸, V. Chulikov³⁸, P. Ciambrone²³, M.F. Cicala⁵⁶, X. Cid Vidal⁴⁶, G. Ciezarek⁴⁸,
 P.E.L. Clarke⁵⁸, M. Clemencic⁴⁸, H.V. Cliff⁵⁵, J. Closier⁴⁸, J.L. Cobbedick⁶², V. Coco⁴⁸,
 J.A.B. Coelho¹¹, J. Cogan¹⁰, E. Cogneras⁹, L. Cojocariu³⁷, P. Collins⁴⁸, T. Colombo⁴⁸,
 L. Congedo^{19,c}, A. Contu²⁷, N. Cooke⁵³, G. Coombs⁵⁹, G. Corti⁴⁸, C.M. Costa Sobral⁵⁶,
 B. Couturier⁴⁸, D.C. Craik⁶⁴, J. Crkovská⁶⁷, M. Cruz Torres¹, R. Currie⁵⁸, C.L. Da Silva⁶⁷,
 S. Dadabaev⁸³, E. Dall'Occo¹⁵, J. Dalseno⁴⁶, C. D'Ambrosio⁴⁸, A. Danilina⁴¹, P. d'Argent⁴⁸,
 A. Davis⁶², O. De Aguiar Francisco⁶², K. De Bruyn⁷⁹, S. De Capua⁶², M. De Cian⁴⁹,
 J.M. De Miranda¹, L. De Paula², M. De Serio^{19,c}, D. De Simone⁵⁰, P. De Simone²³,
 J.A. de Vries⁸⁰, C.T. Dean⁶⁷, D. Decamp⁸, L. Del Buono¹³, B. Delaney⁵⁵, H.-P. Dembinski¹⁵,
 A. Dendek³⁴, V. Denysenko⁵⁰, D. Derkach⁸², O. Deschamps⁹, F. Desse¹¹, F. Dettori^{27,e},
 B. Dey⁷⁷, A. Di Canto⁴⁸, A. Di Cicco²³, P. Di Nezza²³, S. Didenko⁸³, L. Dieste Maronas⁴⁶,
 H. Dijkstra⁴⁸, V. Dobishuk⁵², A.M. Donohoe¹⁸, F. Dordei²⁷, A.C. dos Reis¹, L. Douglas⁵⁹,
 A. Dovbnya⁵¹, A.G. Downes⁸, K. Dreimanis⁶⁰, M.W. Dudek³⁵, L. Dufour⁴⁸, V. Duk⁷⁸,
 P. Durante⁴⁸, J.M. Durham⁶⁷, D. Dutta⁶², A. Dziurda³⁵, A. Dzyuba³⁸, S. Easo⁵⁷, U. Egede⁶⁹,
 V. Egorychev⁴¹, S. Eidelman^{43,v}, S. Eisenhardt⁵⁸, S. Ek-In⁴⁹, L. Eklund^{59,w}, S. Ely⁶⁸, A. Ene³⁷,
 E. Epple⁶⁷, S. Escher¹⁴, J. Eschle⁵⁰, S. Esen¹³, T. Evans⁴⁸, A. Falabella²⁰, J. Fan³, Y. Fan⁶,
 B. Fang⁷³, S. Farry⁶⁰, D. Fazzini^{26,j}, M. Féo⁴⁸, A. Fernandez Prieto⁴⁶,
 J.M. Fernandez-tenllado Arribas⁴⁵, A.D. Fernez⁶⁶, F. Ferrari^{20,d}, L. Ferreira Lopes⁴⁹,
 F. Ferreira Rodrigues², S. Ferreres Sole³², M. Ferrillo⁵⁰, M. Ferro-Luzzi⁴⁸, S. Filippov³⁹,
 R.A. Fini¹⁹, M. Fiorini^{21,f}, M. Firlej³⁴, K.M. Fischer⁶³, D.S. Fitzgerald⁸⁶, C. Fitzpatrick⁶²,
 T. Fiutowski³⁴, A. Fkiaras⁴⁸, F. Fleuret¹², M. Fontana¹³, F. Fontanelli^{24,h}, R. Forty⁴⁸,
 V. Franco Lima⁶⁰, M. Franco Sevilla⁶⁶, M. Frank⁴⁸, E. Franzoso²¹, G. Frau¹⁷, C. Frei⁴⁸,

D.A. Friday⁵⁹, J. Fu²⁵, Q. Fuehring¹⁵, W. Funk⁴⁸, E. Gabriel³², T. Gaintseva⁴²,
 A. Gallas Torreira⁴⁶, D. Galli^{20,d}, S. Gambetta^{58,48}, Y. Gan³, M. Gandelman², P. Gandini²⁵,
 Y. Gao⁵, M. Garau²⁷, L.M. Garcia Martin⁵⁶, P. Garcia Moreno⁴⁵, J. García Pardiñas^{26,j},
 B. Garcia Plana⁴⁶, F.A. Garcia Rosales¹², L. Garrido⁴⁵, C. Gaspar⁴⁸, R.E. Geertsema³²,
 D. Gerick¹⁷, L.L. Gerken¹⁵, E. Gersabeck⁶², M. Gersabeck⁶², T. Gershon⁵⁶, D. Gerstel¹⁰,
 Ph. Ghez⁸, V. Gibson⁵⁵, H.K. Giemza³⁶, M. Giovannetti^{23,p}, A. Gioventù⁴⁶,
 P. Gironella Gironell⁴⁵, L. Giubega³⁷, C. Giugliano^{21,f,48}, K. Gizdov⁵⁸, E.L. Gkougkousis⁴⁸,
 V.V. Gligorov¹³, C. Göbel⁷⁰, E. Golobardes⁸⁵, D. Golubkov⁴¹, A. Golutvin^{61,83}, A. Gomes^{1,a},
 S. Gomez Fernandez⁴⁵, F. Goncalves Abrantes⁶³, M. Goncerz³⁵, G. Gong³, P. Gorbounov⁴¹,
 I.V. Gorelov⁴⁰, C. Gotti²⁶, E. Govorkova⁴⁸, J.P. Grabowski¹⁷, T. Grammatico¹³,
 L.A. Granado Cardoso⁴⁸, E. Graugés⁴⁵, E. Graverini⁴⁹, G. Graziani²², A. Grecu³⁷,
 L.M. Greeven³², P. Griffith^{21,f}, L. Grillo⁶², S. Gromov⁸³, B.R. Gruberg Cazon⁶³, C. Gu³,
 M. Guarise²¹, P. A. Günther¹⁷, E. Gushchin³⁹, A. Guth¹⁴, Y. Guz⁴⁴, T. Gys⁴⁸,
 T. Hadavizadeh⁶⁹, G. Haefeli⁴⁹, C. Haen⁴⁸, J. Haimberger⁴⁸, T. Halewood-leagas⁶⁰,
 P.M. Hamilton⁶⁶, J.P. Hammerich⁶⁰, Q. Han⁷, X. Han¹⁷, T.H. Hancock⁶³,
 S. Hansmann-Menzemer¹⁷, N. Harnew⁶³, T. Harrison⁶⁰, C. Hasse⁴⁸, M. Hatch⁴⁸, J. He^{6,b},
 M. Hecker⁶¹, K. Heijhoff³², K. Heinicke¹⁵, A.M. Hennequin⁴⁸, K. Hennessy⁶⁰, L. Henry⁴⁸,
 J. Heuel¹⁴, A. Hicheur², D. Hill⁴⁹, M. Hilton⁶², S.E. Hollitt¹⁵, J. Hu¹⁷, J. Hu⁷², W. Hu⁷,
 X. Hu³, W. Huang⁶, X. Huang⁷³, W. Hulsbergen³², R.J. Hunter⁵⁶, M. Hushchyn⁸²,
 D. Hutchcroft⁶⁰, D. Hynds³², P. Ibis¹⁵, M. Idzik³⁴, D. Ilin³⁸, P. Ilten⁶⁵, A. Inglessi³⁸,
 A. Ishteev⁸³, K. Ivshin³⁸, R. Jacobsson⁴⁸, S. Jakobsen⁴⁸, E. Jans³², B.K. Jashal⁴⁷,
 A. Jawahery⁶⁶, V. Jevtic¹⁵, M. Jezabek³⁵, F. Jiang³, M. John⁶³, D. Johnson⁴⁸, C.R. Jones⁵⁵,
 T.P. Jones⁵⁶, B. Jost⁴⁸, N. Jurik⁴⁸, S. Kandybei⁵¹, Y. Kang³, M. Karacson⁴⁸, M. Karpov⁸²,
 F. Keizer⁴⁸, M. Kenzie⁵⁶, T. Ketel³³, B. Khanji¹⁵, A. Kharisova⁸⁴, S. Kholodenko⁴⁴, T. Kirm¹⁴,
 V.S. Kirsebom⁴⁹, O. Kitouni⁶⁴, S. Klaver³², K. Klimaszewski³⁶, S. Koliiev⁵², A. Kondybayeva⁸³,
 A. Konoplyannikov⁴¹, P. Kopciwicz³⁴, R. Kopecna¹⁷, P. Koppenburg³², M. Korolev⁴⁰,
 I. Kostyuk^{32,52}, O. Kot⁵², S. Kotriakhova^{21,38}, P. Kravchenko³⁸, L. Kravchuk³⁹,
 R.D. Krawczyk⁴⁸, M. Kreps⁵⁶, F. Kress⁶¹, S. Kretzschmar¹⁴, P. Krokovny^{43,v}, W. Krupa³⁴,
 W. Krzemien³⁶, W. Kucewicz^{35,t}, M. Kucharczyk³⁵, V. Kudryavtsev^{43,v}, H.S. Kuindersma^{32,33},
 G.J. Kunde⁶⁷, T. Kvaratskheliya⁴¹, D. Lacarrere⁴⁸, G. Lafferty⁶², A. Lai²⁷, A. Lampis²⁷,
 D. Lancierini⁵⁰, J.J. Lane⁶², R. Lane⁵⁴, G. Lanfranchi²³, C. Langenbruch¹⁴, J. Langer¹⁵,
 O. Lantwin⁵⁰, T. Latham⁵⁶, F. Lazzari^{29,q}, R. Le Gac¹⁰, S.H. Lee⁸⁶, R. Lefèvre⁹, A. Leflat⁴⁰,
 S. Legotin⁸³, O. Leroy¹⁰, T. Lesiak³⁵, B. Leverington¹⁷, H. Li⁷², L. Li⁶³, P. Li¹⁷, S. Li⁷, Y. Li⁴,
 Y. Li⁴, Z. Li⁶⁸, X. Liang⁶⁸, T. Lin⁶¹, R. Lindner⁴⁸, V. Lisovskyi¹⁵, R. Litvinov²⁷, G. Liu⁷²,
 H. Liu⁶, S. Liu⁴, A. Loi²⁷, J. Lomba Castro⁴⁶, I. Longstaff⁵⁹, J.H. Lopes², G.H. Lovell⁵⁵, Y. Lu⁴,
 D. Lucchesi^{28,l}, S. Luchuk³⁹, M. Lucio Martinez³², V. Lukashenko³², Y. Luo³, A. Lupato⁶²,
 E. Luppi^{21,f}, O. Lupton⁵⁶, A. Lusiani^{29,m}, X. Lyu⁶, L. Ma⁴, R. Ma⁶, S. Maccolini^{20,d},
 F. Machefert¹¹, F. Maciuc³⁷, V. Macko⁴⁹, P. Mackowiak¹⁵, S. Maddrell-Mander⁵⁴,
 O. Madejczyk³⁴, L.R. Madhan Mohan⁵⁴, O. Maev³⁸, A. Maevskiy⁸², D. Maisuzenko³⁸,
 M.W. Majewski³⁴, J.J. Malczewski³⁵, S. Malde⁶³, B. Malecki⁴⁸, A. Malinin⁸¹, T. Maltsev^{43,v},
 H. Malygina¹⁷, G. Manca^{27,e}, G. Mancinelli¹⁰, D. Manuzzi^{20,d}, D. Marangotto^{25,i}, J. Maratas^{9,s},
 J.F. Marchand⁸, U. Marconi²⁰, S. Mariani^{22,g}, C. Marin Benito⁴⁸, M. Marinangeli⁴⁹, J. Marks¹⁷,
 A.M. Marshall⁵⁴, P.J. Marshall⁶⁰, G. Martellotti³⁰, L. Martinazzoli^{48,j}, M. Martinelli^{26,j},
 D. Martinez Santos⁴⁶, F. Martinez Vidal⁴⁷, A. Massafferri¹, M. Materok¹⁴, R. Matev⁴⁸,
 A. Mathad⁵⁰, Z. Mathe⁴⁸, V. Matiunin⁴¹, C. Matteuzzi²⁶, K.R. Mattioli⁸⁶, A. Mauri³²,
 E. Maurice¹², J. Mauricio⁴⁵, M. Mazurek⁴⁸, M. McCann⁶¹, L. Mcconnell¹⁸, T.H. Mcgrath⁶²,
 A. McNab⁶², R. McNulty¹⁸, J.V. Mead⁶⁰, B. Meadows⁶⁵, G. Meier¹⁵, N. Meinert⁷⁶,
 D. Melnychuk³⁶, S. Meloni^{26,j}, M. Merk^{32,80}, A. Merli²⁵, L. Meyer Garcia², M. Mikhasenko⁴⁸,
 D.A. Milanese⁷⁴, E. Millard⁵⁶, M. Milovanovic⁴⁸, M.-N. Minard⁸, A. Minotti²¹, L. Minzoni^{21,f},
 S.E. Mitchell⁵⁸, B. Mitreska⁶², D.S. Mitzel⁴⁸, A. Mödden¹⁵, R.A. Mohammed⁶³, R.D. Moise⁶¹,

T. Mombächer⁴⁶, I.A. Monroy⁷⁴, S. Monteil⁹, M. Morandin²⁸, G. Morello²³, M.J. Morello^{29,m},
 J. Moron³⁴, A.B. Morris⁷⁵, A.G. Morris⁵⁶, R. Mountain⁶⁸, H. Mu³, F. Muheim^{58,48},
 M. Mulder⁴⁸, D. Müller⁴⁸, K. Müller⁵⁰, C.H. Murphy⁶³, D. Murray⁶², P. Muzzetto^{27,48},
 P. Naik⁵⁴, T. Nakada⁴⁹, R. Nandakumar⁵⁷, T. Nanut⁴⁹, I. Nasteva², M. Needham⁵⁸, I. Neri²¹,
 N. Neri^{25,i}, S. Neubert⁷⁵, N. Neufeld⁴⁸, R. Newcombe⁶¹, T.D. Nguyen⁴⁹, C. Nguyen-Mau^{49,x},
 E.M. Niel¹¹, S. Nieswand¹⁴, N. Nikitin⁴⁰, N.S. Nolte⁶⁴, C. Normand⁸, C. Nunez⁸⁶,
 A. Oblakowska-Mucha³⁴, V. Obraztsov⁴⁴, D.P. O’Hanlon⁵⁴, R. Oldeman^{27,e}, M.E. Olivares⁶⁸,
 C.J.G. Onderwater⁷⁹, R.H. O’neil⁵⁸, A. Ossowska³⁵, J.M. Otalora Goicochea²,
 T. Ovsianikova⁴¹, P. Owen⁵⁰, A. Oyanguren⁴⁷, B. Pagare⁵⁶, P.R. Pais⁴⁸, T. Pajero⁶³,
 A. Palano¹⁹, M. Palutan²³, Y. Pan⁶², G. Panshin⁸⁴, A. Papanestis⁵⁷, M. Pappagallo^{19,c},
 L.L. Pappalardo^{21,f}, C. Pappenheimer⁶⁵, W. Parker⁶⁶, C. Parkes⁶², C.J. Parkinson⁴⁶,
 B. Passalacqua²¹, G. Passaleva²², A. Pastore¹⁹, M. Patel⁶¹, C. Patrignani^{20,d}, C.J. Pawley⁸⁰,
 A. Pearce⁴⁸, A. Pellegrino³², M. Pepe Altarelli⁴⁸, S. Perazzini²⁰, D. Pereima⁴¹, P. Perret⁹,
 I. Petrenko⁵², M. Petric^{59,48}, K. Petridis⁵⁴, A. Petrolini^{24,h}, A. Petrov⁸¹, S. Petrucci⁵⁸,
 M. Petruzzo²⁵, T.T.H. Pham⁶⁸, A. Philippov⁴², L. Pica^{29,m}, M. Piccini⁷⁸, B. Pietrzyk⁸,
 G. Pietrzyk⁴⁹, M. Pili⁶³, D. Pinci³⁰, F. Pisani⁴⁸, Resmi P.K¹⁰, V. Placinta³⁷, J. Plews⁵³,
 M. Plo Casasus⁴⁶, F. Polci¹³, M. Poli Lener²³, M. Poliakov⁶⁸, A. Poluektov¹⁰, N. Polukhina^{83,u},
 I. Polyakov⁶⁸, E. Polycarpo², G.J. Pomery⁵⁴, S. Ponce⁴⁸, D. Popov^{6,48}, S. Popov⁴²,
 S. Poslavskii⁴⁴, K. Prasanth³⁵, L. Promberger⁴⁸, C. Prouve⁴⁶, V. Pugatch⁵², H. Pullen⁶³,
 G. Punzi^{29,n}, H. Qi³, W. Qian⁶, J. Qin⁶, N. Qin³, R. Quagliani¹³, B. Quintana⁸, N.V. Raab¹⁸,
 R.I. Rabadan Trejo¹⁰, B. Rachwal³⁴, J.H. Rademacker⁵⁴, M. Rama²⁹, M. Ramos Pernas⁵⁶,
 M.S. Rangel², F. Ratnikov^{42,82}, G. Raven³³, M. Reboud⁸, F. Redi⁴⁹, F. Reiss⁶²,
 C. Remon Alepuz⁴⁷, Z. Ren³, V. Renaudin⁶³, R. Ribatti²⁹, S. Ricciardi⁵⁷, K. Rinnert⁶⁰,
 P. Robbe¹¹, G. Robertson⁵⁸, A.B. Rodrigues⁴⁹, E. Rodrigues⁶⁰, J.A. Rodriguez Lopez⁷⁴,
 A. Rollings⁶³, P. Roloff⁴⁸, V. Romanovskiy⁴⁴, M. Romero Lamas⁴⁶, A. Romero Vidal⁴⁶,
 J.D. Roth⁸⁶, M. Rotondo²³, M.S. Rudolph⁶⁸, T. Ruf⁴⁸, J. Ruiz Vidal⁴⁷, A. Ryzhikov⁸²,
 J. Ryzka³⁴, J.J. Saborido Silva⁴⁶, N. Sagidova³⁸, N. Sahoo⁵⁶, B. Saitta^{27,e}, M. Salomoni⁴⁸,
 D. Sanchez Gonzalo⁴⁵, C. Sanchez Gras³², R. Santacesaria³⁰, C. Santamarina Rios⁴⁶,
 M. Santimaria²³, E. Santovetti^{31,p}, D. Saranin⁸³, G. Sarpis⁵⁹, M. Sarpis⁷⁵, A. Sarti³⁰,
 C. Satriano^{30,o}, A. Satta³¹, M. Saur¹⁵, D. Savrina^{41,40}, H. Sazak⁹, L.G. Scantlebury Smead⁶³,
 A. Scarabotto¹³, S. Schael¹⁴, M. Schiller⁵⁹, H. Schindler⁴⁸, M. Schmelling¹⁶, B. Schmidt⁴⁸,
 O. Schneider⁴⁹, A. Schopper⁴⁸, M. Schubiger³², S. Schulte⁴⁹, M.H. Schune¹¹, R. Schwemmer⁴⁸,
 B. Sciascia²³, S. Sellam⁴⁶, A. Semennikov⁴¹, M. Senghi Soares³³, A. Sergi²⁴, N. Serra⁵⁰,
 L. Sestini²⁸, A. Seuthe¹⁵, P. Seyfert⁴⁸, Y. Shang⁵, D.M. Shangase⁸⁶, M. Shapkin⁴⁴,
 I. Shchemerov⁸³, L. Shchutska⁴⁹, T. Shears⁶⁰, L. Shekhtman^{43,v}, Z. Shen⁵, V. Shevchenko⁸¹,
 E.B. Shields^{26,j}, E. Shmanin⁸³, J.D. Shupperd⁶⁸, B.G. Siddi²¹, R. Silva Coutinho⁵⁰, G. Simi²⁸,
 S. Simone^{19,c}, N. Skidmore⁶², T. Skwarnicki⁶⁸, M.W. Slater⁵³, I. Slazyk^{21,f}, J.C. Smallwood⁶³,
 J.G. Smeaton⁵⁵, A. Smetkina⁴¹, E. Smith⁵⁰, M. Smith⁶¹, A. Snoch³², M. Soares²⁰,
 L. Soares Lavra⁹, M.D. Sokoloff⁶⁵, F.J.P. Soler⁵⁹, A. Solovov³⁸, I. Solovyev³⁸,
 F.L. Souza De Almeida², B. Souza De Paula², B. Spaan¹⁵, E. Spadaro Norella^{25,i}, P. Spradlin⁵⁹,
 F. Stagni⁴⁸, M. Stahl⁶⁵, S. Stahl⁴⁸, P. Stefko⁴⁹, O. Steinkamp^{50,83}, O. Stenyakin⁴⁴, H. Stevens¹⁵,
 S. Stone⁶⁸, M.E. Stramaglia⁴⁹, M. Straticiu³⁷, D. Strelakina⁸³, F. Suljik⁶³, J. Sun²⁷, L. Sun⁷³,
 Y. Sun⁶⁶, P. Svihra⁶², P.N. Swallow⁵³, K. Swientek³⁴, A. Szabelski³⁶, T. Szumlak³⁴,
 M. Szymanski⁴⁸, S. Taneja⁶², A.R. Tanner⁵⁴, A. Terentev⁸³, F. Teubert⁴⁸, E. Thomas⁴⁸,
 K.A. Thomson⁶⁰, V. Tisserand⁹, S. T’Jampens⁸, M. Tobin⁴, L. Tomassetti^{21,f},
 D. Torres Machado¹, D.Y. Tou¹³, M.T. Tran⁴⁹, E. Trifonova⁸³, C. Trippi⁴⁹, G. Tuci^{29,n},
 A. Tully⁴⁹, N. Tuning^{32,48}, A. Ukleja³⁶, D.J. Unverzagt¹⁷, E. Ursov⁸³, A. Usachov³²,
 A. Ustyuzhanin^{42,82}, U. Uwer¹⁷, A. Vagner⁸⁴, V. Vagnoni²⁰, A. Valassi⁴⁸, G. Valenti²⁰,
 N. Valls Canudas⁸⁵, M. van Beuzekom³², M. Van Dijk⁴⁹, E. van Herwijnen⁸³, C.B. Van Hulse¹⁸,
 M. van Veghel⁷⁹, R. Vazquez Gomez⁴⁶, P. Vazquez Regueiro⁴⁶, C. Vázquez Sierra⁴⁸, S. Vecchi²¹,

J.J. Velthuis⁵⁴, M. Veltri^{22,r}, A. Venkateswaran⁶⁸, M. Veronesi³², M. Vesterinen⁵⁶, D. Vieira⁶⁵, M. Vieites Diaz⁴⁹, H. Viemann⁷⁶, X. Vilasis-Cardona⁸⁵, E. Vilella Figueras⁶⁰, A. Villa²⁰, P. Vincent¹³, D. Vom Bruch¹⁰, A. Vorobyev³⁸, V. Vorobyev^{43,v}, N. Voropaev³⁸, K. Vos⁸⁰, R. Waldi¹⁷, J. Walsh²⁹, C. Wang¹⁷, J. Wang⁵, J. Wang⁴, J. Wang³, J. Wang⁷³, M. Wang³, R. Wang⁵⁴, Y. Wang⁷, Z. Wang⁵⁰, Z. Wang³, H.M. Wark⁶⁰, N.K. Watson⁵³, S.G. Weber¹³, D. Websdale⁶¹, C. Weisser⁶⁴, B.D.C. Westhenry⁵⁴, D.J. White⁶², M. Whitehead⁵⁴, D. Wiedner¹⁵, G. Wilkinson⁶³, M. Wilkinson⁶⁸, I. Williams⁵⁵, M. Williams⁶⁴, M.R.J. Williams⁵⁸, F.F. Wilson⁵⁷, W. Wislicki³⁶, M. Witek³⁵, L. Witola¹⁷, G. Wormser¹¹, S.A. Wotton⁵⁵, H. Wu⁶⁸, K. Wyllie⁴⁸, Z. Xiang⁶, D. Xiao⁷, Y. Xie⁷, A. Xu⁵, J. Xu⁶, L. Xu³, M. Xu⁷, Q. Xu⁶, Z. Xu⁵, Z. Xu⁶, D. Yang³, S. Yang⁶, Y. Yang⁶, Z. Yang³, Z. Yang⁶⁶, Y. Yao⁶⁸, L.E. Yeomans⁶⁰, H. Yin⁷, J. Yu⁷¹, X. Yuan⁶⁸, O. Yushchenko⁴⁴, E. Zaffaroni⁴⁹, M. Zavertyaev^{16,u}, M. Zdybal³⁵, O. Zenaiev⁴⁸, M. Zeng³, D. Zhang⁷, L. Zhang³, S. Zhang⁵, Y. Zhang⁵, Y. Zhang⁶³, A. Zharkova⁸³, A. Zhelezov¹⁷, Y. Zheng⁶, X. Zhou⁶, Y. Zhou⁶, X. Zhu³, Z. Zhu⁶, V. Zhukov^{14,40}, J.B. Zonneveld⁵⁸, Q. Zou⁴, S. Zucchelli^{20,d}, D. Zuliani²⁸, G. Zunica⁶².

¹Centro Brasileiro de Pesquisas Físicas (CBPF), Rio de Janeiro, Brazil

²Universidade Federal do Rio de Janeiro (UFRJ), Rio de Janeiro, Brazil

³Center for High Energy Physics, Tsinghua University, Beijing, China

⁴Institute Of High Energy Physics (IHEP), Beijing, China

⁵School of Physics State Key Laboratory of Nuclear Physics and Technology, Peking University, Beijing, China

⁶University of Chinese Academy of Sciences, Beijing, China

⁷Institute of Particle Physics, Central China Normal University, Wuhan, Hubei, China

⁸Univ. Savoie Mont Blanc, CNRS, IN2P3-LAPP, Annecy, France

⁹Université Clermont Auvergne, CNRS/IN2P3, LPC, Clermont-Ferrand, France

¹⁰Aix Marseille Univ, CNRS/IN2P3, CPPM, Marseille, France

¹¹Université Paris-Saclay, CNRS/IN2P3, IJCLab, Orsay, France

¹²Laboratoire Leprince-Ringuet, CNRS/IN2P3, Ecole Polytechnique, Institut Polytechnique de Paris, Palaiseau, France

¹³LPNHE, Sorbonne Université, Paris Diderot Sorbonne Paris Cité, CNRS/IN2P3, Paris, France

¹⁴I. Physikalisches Institut, RWTH Aachen University, Aachen, Germany

¹⁵Fakultät Physik, Technische Universität Dortmund, Dortmund, Germany

¹⁶Max-Planck-Institut für Kernphysik (MPIK), Heidelberg, Germany

¹⁷Physikalisches Institut, Ruprecht-Karls-Universität Heidelberg, Heidelberg, Germany

¹⁸School of Physics, University College Dublin, Dublin, Ireland

¹⁹INFN Sezione di Bari, Bari, Italy

²⁰INFN Sezione di Bologna, Bologna, Italy

²¹INFN Sezione di Ferrara, Ferrara, Italy

²²INFN Sezione di Firenze, Firenze, Italy

²³INFN Laboratori Nazionali di Frascati, Frascati, Italy

²⁴INFN Sezione di Genova, Genova, Italy

²⁵INFN Sezione di Milano, Milano, Italy

²⁶INFN Sezione di Milano-Bicocca, Milano, Italy

²⁷INFN Sezione di Cagliari, Monserrato, Italy

²⁸Università degli Studi di Padova, Università e INFN, Padova, Padova, Italy

²⁹INFN Sezione di Pisa, Pisa, Italy

³⁰INFN Sezione di Roma La Sapienza, Roma, Italy

³¹INFN Sezione di Roma Tor Vergata, Roma, Italy

³²Nikhef National Institute for Subatomic Physics, Amsterdam, Netherlands

³³Nikhef National Institute for Subatomic Physics and VU University Amsterdam, Amsterdam, Netherlands

³⁴AGH - University of Science and Technology, Faculty of Physics and Applied Computer Science, Kraków, Poland

³⁵Henryk Niewodniczanski Institute of Nuclear Physics Polish Academy of Sciences, Kraków, Poland

³⁶National Center for Nuclear Research (NCBJ), Warsaw, Poland

- ³⁷ Horia Hulubei National Institute of Physics and Nuclear Engineering, Bucharest-Magurele, Romania
- ³⁸ Petersburg Nuclear Physics Institute NRC Kurchatov Institute (PNPI NRC KI), Gatchina, Russia
- ³⁹ Institute for Nuclear Research of the Russian Academy of Sciences (INR RAS), Moscow, Russia
- ⁴⁰ Institute of Nuclear Physics, Moscow State University (SINP MSU), Moscow, Russia
- ⁴¹ Institute of Theoretical and Experimental Physics NRC Kurchatov Institute (ITEP NRC KI), Moscow, Russia
- ⁴² Yandex School of Data Analysis, Moscow, Russia
- ⁴³ Budker Institute of Nuclear Physics (SB RAS), Novosibirsk, Russia
- ⁴⁴ Institute for High Energy Physics NRC Kurchatov Institute (IHEP NRC KI), Protvino, Russia, Protvino, Russia
- ⁴⁵ ICCUB, Universitat de Barcelona, Barcelona, Spain
- ⁴⁶ Instituto Galego de Física de Altas Enerxías (IGFAE), Universidade de Santiago de Compostela, Santiago de Compostela, Spain
- ⁴⁷ Instituto de Física Corpuscular, Centro Mixto Universidad de Valencia - CSIC, Valencia, Spain
- ⁴⁸ European Organization for Nuclear Research (CERN), Geneva, Switzerland
- ⁴⁹ Institute of Physics, Ecole Polytechnique Fédérale de Lausanne (EPFL), Lausanne, Switzerland
- ⁵⁰ Physik-Institut, Universität Zürich, Zürich, Switzerland
- ⁵¹ NSC Kharkiv Institute of Physics and Technology (NSC KIPT), Kharkiv, Ukraine
- ⁵² Institute for Nuclear Research of the National Academy of Sciences (KINR), Kyiv, Ukraine
- ⁵³ University of Birmingham, Birmingham, United Kingdom
- ⁵⁴ H.H. Wills Physics Laboratory, University of Bristol, Bristol, United Kingdom
- ⁵⁵ Cavendish Laboratory, University of Cambridge, Cambridge, United Kingdom
- ⁵⁶ Department of Physics, University of Warwick, Coventry, United Kingdom
- ⁵⁷ STFC Rutherford Appleton Laboratory, Didcot, United Kingdom
- ⁵⁸ School of Physics and Astronomy, University of Edinburgh, Edinburgh, United Kingdom
- ⁵⁹ School of Physics and Astronomy, University of Glasgow, Glasgow, United Kingdom
- ⁶⁰ Oliver Lodge Laboratory, University of Liverpool, Liverpool, United Kingdom
- ⁶¹ Imperial College London, London, United Kingdom
- ⁶² Department of Physics and Astronomy, University of Manchester, Manchester, United Kingdom
- ⁶³ Department of Physics, University of Oxford, Oxford, United Kingdom
- ⁶⁴ Massachusetts Institute of Technology, Cambridge, MA, United States
- ⁶⁵ University of Cincinnati, Cincinnati, OH, United States
- ⁶⁶ University of Maryland, College Park, MD, United States
- ⁶⁷ Los Alamos National Laboratory (LANL), Los Alamos, United States
- ⁶⁸ Syracuse University, Syracuse, NY, United States
- ⁶⁹ School of Physics and Astronomy, Monash University, Melbourne, Australia, associated to ⁵⁶
- ⁷⁰ Pontifícia Universidade Católica do Rio de Janeiro (PUC-Rio), Rio de Janeiro, Brazil, associated to ²
- ⁷¹ Physics and Micro Electronic College, Hunan University, Changsha City, China, associated to ⁷
- ⁷² Guangdong Provincial Key Laboratory of Nuclear Science, Guangdong-Hong Kong Joint Laboratory of Quantum Matter, Institute of Quantum Matter, South China Normal University, Guangzhou, China, associated to ³
- ⁷³ School of Physics and Technology, Wuhan University, Wuhan, China, associated to ³
- ⁷⁴ Departamento de Física, Universidad Nacional de Colombia, Bogota, Colombia, associated to ¹³
- ⁷⁵ Universität Bonn - Helmholtz-Institut für Strahlen und Kernphysik, Bonn, Germany, associated to ¹⁷
- ⁷⁶ Institut für Physik, Universität Rostock, Rostock, Germany, associated to ¹⁷
- ⁷⁷ Eotvos Lorand University, Budapest, Hungary, associated to ⁴⁸
- ⁷⁸ INFN Sezione di Perugia, Perugia, Italy, associated to ²¹
- ⁷⁹ Van Swinderen Institute, University of Groningen, Groningen, Netherlands, associated to ³²
- ⁸⁰ Universiteit Maastricht, Maastricht, Netherlands, associated to ³²
- ⁸¹ National Research Centre Kurchatov Institute, Moscow, Russia, associated to ⁴¹
- ⁸² National Research University Higher School of Economics, Moscow, Russia, associated to ⁴²
- ⁸³ National University of Science and Technology "MISIS", Moscow, Russia, associated to ⁴¹
- ⁸⁴ National Research Tomsk Polytechnic University, Tomsk, Russia, associated to ⁴¹
- ⁸⁵ DS4DS, La Salle, Universitat Ramon Llull, Barcelona, Spain, associated to ⁴⁵
- ⁸⁶ University of Michigan, Ann Arbor, United States, associated to ⁶⁸

^a Universidade Federal do Triângulo Mineiro (UFTM), Uberaba-MG, Brazil

- ^bHangzhou Institute for Advanced Study, UCAS, Hangzhou, China
^cUniversità di Bari, Bari, Italy
^dUniversità di Bologna, Bologna, Italy
^eUniversità di Cagliari, Cagliari, Italy
^fUniversità di Ferrara, Ferrara, Italy
^gUniversità di Firenze, Firenze, Italy
^hUniversità di Genova, Genova, Italy
ⁱUniversità degli Studi di Milano, Milano, Italy
^jUniversità di Milano Bicocca, Milano, Italy
^kUniversità di Modena e Reggio Emilia, Modena, Italy
^lUniversità di Padova, Padova, Italy
^mScuola Normale Superiore, Pisa, Italy
ⁿUniversità di Pisa, Pisa, Italy
^oUniversità della Basilicata, Potenza, Italy
^pUniversità di Roma Tor Vergata, Roma, Italy
^qUniversità di Siena, Siena, Italy
^rUniversità di Urbino, Urbino, Italy
^sMSU - Iligan Institute of Technology (MSU-IIT), Iligan, Philippines
^tAGH - University of Science and Technology, Faculty of Computer Science, Electronics and Telecommunications, Kraków, Poland
^uP.N. Lebedev Physical Institute, Russian Academy of Science (LPI RAS), Moscow, Russia
^vNovosibirsk State University, Novosibirsk, Russia
^wDepartment of Physics and Astronomy, Uppsala University, Uppsala, Sweden
^xHanoi University of Science, Hanoi, Vietnam